Dalton Transactions

PAPER

View Article Online
View Journal | View Issue

Cite this: *Dalton Trans.*, 2017, **46**, 16096

Highly selective adsorption of *p*-xylene over other C_8 aromatic hydrocarbons by Co-CUK-1: a combined experimental and theoretical assessment†

Ji Woong Yoon,‡[a] Ji Sun Lee,‡[a,b] Graham W. Piburn,[c] Kyoung Ho Cho,[a] Keonghee Jeon,[d] Hyung-Kyu Lim,[d] Hyungjun Kim,[d] Chul-Ho Jun,[b] Simon M. Humphrey,*[c] Rajamani Krishna*[e] and Jong-San Chang*[a,f]

Received 5th September 2017,
Accepted 19th October 2017

DOI: 10.1039/c7dt03304d

rsc.li/dalton

High quality crystalline Co-CUK-1 can be synthesized rapidly and efficiently by a microwave-assisted method. The resulting microporous coordination material is a highly effective adsorbent for the separation of xylene isomers and ethylbenzene, as demonstrated here through sorption isotherm analysis, Ideal Adsorbed Solution Theory (IAST) calculations, and grand canonical Monte Carlo (GCMC) simulations. Co-CUK-1 showed high sorption capacity and high adsorption selectivity for *p*-xylene over the corresponding *m*- and *o*-isomers, and ethylbenzenes. According to the data obtained from IAST and GCMC simulations, the Co-CUK-1 is found to strongly favour *p*-xylene adsorption because *p*-xylene molecules undergo well-defined molecular packing in the 1-D channels; by comparison, the packing efficiencies of *o*-xylene, *m*-xylene and ethylbenzene are significantly lower, as is evidenced by lower saturation capacities.

1. Introduction

para-Xylene is a valuable petrochemical feedstock employed in the production of polyethylene terephthalate (PET), which is one of the largest volume polymers in the world. In a commonly used separation scheme employed in the petrochemical industry, a xylene-rich stream fed from the bottom of a reformer splitter is routed into a xylene splitter. Heavier aromatics (C_{9+}) are removed from the bottom of the column. The overhead stream from the xylene splitter, typically containing 19% ethylbenzene, 44% *m*-xylene, 20% *o*-xylene, and 17% *p*-xylene, needs to be separated to allow for recovery of pure *p*-xylene. Currently, this mixture is separated in a Simulated Moving Bed (SMB) separation unit, using zeolitic adsorbents such as BaX zeolite as the stationary phase, which selectively adsorbs *p*-xylene. The industrial separation of xylene isomers is conducted on bulk liquid phase mixtures; under such conditions the pores of BaX are saturated with guest molecules.[1] There is a clear economic incentive for the replacement of zeolites with designer metal–organic framework (MOF) materials, if these can be synthesized with pore architectures that significantly improve the separation performance. If such a MOF is identified, this could lead to an opportunity to develop a more energy-efficient separation protocol for the large-scale production of high purity *p*-xylene.

Porous MOFs are currently of great interest and importance due to their unique sorption properties, which result from inherently high surface areas, controllable pore volumes, and well-ordered pore structures. MOFs also offer the ability to incorporate a broad range of chemical functionalities[2] and the inclusion of a number of different metal elements into their crystalline frameworks.[2] Such properties provide the potential for real applications in the separation of gaseous and/or liquid mixtures.[3] The selective adsorption of *p*-xylene from C_8 aromatic hydrocarbon mixtures is one such feasible application.[4] A viable candidate for this separation application is the previously reported Co-CUK-1, which is comprised of cobalt(II) cations and the dianion of dicarboxylic acid $[Co_3(2,4\text{-pdc})_2(\mu_3\text{-}OH)_2]\cdot 9H_2O$ (2,4-pdc = pyridine-2,4-dicarboxylic acid dianion). The cheap and commercially available components used to prepare Co-CUK-1 are amenable to scaled-up synthesis. This

[a]*Research Center for Nanocatalysts, Korea Research Institute of Chemical Technology (KRICT), P.O. Box 107, Yusung, Daejeon 305-600, Korea. E-mail: jschang@krict.re.kr*
[b]*Department of Chemistry, Center for Bioactive Molecular Hybrid, Yonsei University, Seodamoonku, Seoul 120-749, Korea*
[c]*Department of Chemistry, The University of Texas at Austin, 2.204 Welch Hall, 105 E. 24th St. Stop A5300, Austin, TX 78712, USA. E-mail: smh@cm.utexas.edu*
[d]*Graduate School of Energy, Environment, Water, and Sustainability, Korea Advanced Institute of Science and Technology (KAIST), Daehak-ro 291, Yuseong-gu, Daejeon 305-701, Korea*
[e]*Van't Hoff Institute for Molecular Sciences, University of Amsterdam, Science Park 904, Amsterdam 1098 XH, The Netherland. E-mail: r.krishna@contact.uva.nl*
[f]*Department of Chemistry, Sungkyunkwan University, Suwon 440-476, Korea*
†Electronic supplementary information (ESI) available: Additional calculation details and material characterization. See DOI: 10.1039/c7dt03304d
‡These two authors equally contributed to this work.

unusually stable material incorporates infinite, corrugated 1-D diamond-shaped channels that traverse the structure. The channels are filled with labile guest H_2O molecules of crystallization in its as-synthesized form, but the material is easily dehydrated by heating to 100 °C and/or by treatment in vacuum. The dehydrated phase retains complete crystallinity, as demonstrated from the single-crystal structure of the desolvated material, which was obtained from a diffraction experiment conducted at 375 K and 1 atm (Fig. 1).[5]

Recently, it was reported that a Mg(II)-based isostructural analog, Mg-CUK-1, could be prepared using a microwave-assisted method. Mg-CUK-1 has the unusual ability to selectively adsorb *p*-isomers of xylene and DVB from complex mixtures of isomers; the packing of *p*-xylene molecules was resolved by single-crystal X-ray diffraction of the loaded material.[6] Single-crystal structural elucidation of guest-loaded MOFs is very rare. This information is equally highly valuable, since the results obtained from theoretical models commonly used to predict guest packing orientations may be directly tested against the actual packing orientations observed by X-ray diffraction analysis.

Similar sorption experiments performed using hydrothermally prepared Co-CUK-1 and microwave-synthesized Co-CUK-1 using only H_2O as the solvent are reported here for the first time. Aqueous, microwave-assisted synthesis of functional inorganic materials is highly appealing for scale-up purposes because products can be obtained in minutes rather than hours, and reactions can be conducted under continuous-flow conditions. Somewhat unexpectedly, we show that hydrothermally prepared Co-CUK-1 showed inferior vapour-sorption properties for *p*-xylene at room temperature compared to microwave-prepared material.

We have optimized the microwave-assisted synthesis method for Co-CUK-1, in which a simple purification route provides high quality crystalline solid that is effective in the selective adsorption of C_8 aromatic hydrocarbons. We present experimental data supported by molecular simulations, which demonstrate how Co-CUK-1 obtained from the microwave synthesis route has the desired capability for selective *p*-xylene adsorption. We also demonstrate that Co-CUK-1 has significant advantages over the industrially employed BaX zeolite, both in terms of adsorption selectivity and capacity.

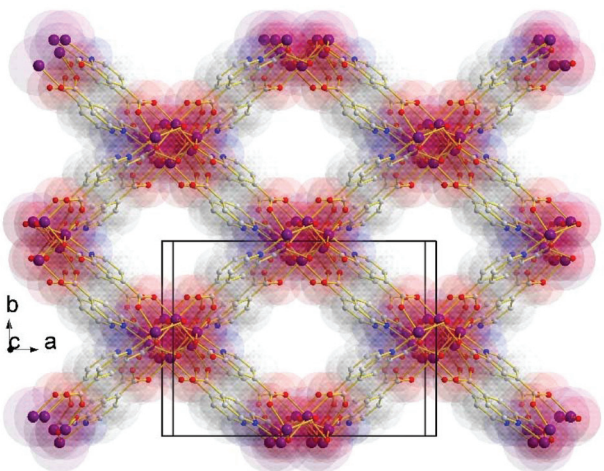

Fig. 1 The extended structure of desolvated Co-CUK-1 obtained by heating a single crystal to 375 K to remove solvent H_2O. The image shows the space-filling model and guest-accessible voids when viewed perpendicular to the direction of propagation of infinite 1-dimensional channels.[5]

2. Experimental section

2.1 Synthesis of Co-CUK-1

Microwave synthesis of Co-CUK-1 (Co-CUK-1(MW)) was carried out using a MARS microwave oven (CEM Corp.). 2,4-Pyridinedicarboxylic acid (1110 mg, 1.0 mmol) and KOH (1.0 M) in H_2O (18.0 cm^3) were added to a stirred solution of $CoCl_2$ hexahydrate (2142 mg, 1.5 mmol) in H_2O (18.0 cm^3) at room temperature to give a viscous, olive-coloured slurry. The slurry was then heated to 473 K for 30 min in the microwave oven inside a 100 cm^3 Teflon-lined Easy-Prep reaction vessel. The reaction temperature was monitored using a fibre-optic sensor. After cooling (30 min), the crystalline solid was purified by brief (3 × 20 s) cycles of sonication in fresh H_2O (100 cm^3), followed by decanting of the cloudy supernatant. Large, pink prismatic crystals were isolated (average yield, 1320 mg). For comparison, hydrothermal synthesis of Co-CUK-1 (Co-CUK-1(HT)) was carried out using a recipe already reported elsewhere.[4] For further purification, the sample was treated with DMF or ethanol under stirring at 343 K for 5 h.

2.2 Characterization of Co-CUK-1

Powder X-ray diffraction patterns of Co-CUK-1 were obtained by Rigaku diffractometer (D/MAX IIIB, 2 kW) using Ni-filtered CuKα-radiation (40 kV, 30 mA, λ = 1.5406 Å) and a graphite crystal monochromator. The particle morphology and crystal size were analyzed by a scanning electron microscope (SEM, Pilips, XL30S FEG). The BET surface area measurements were performed with N_2 adsorption–desorption isotherms at liquid nitrogen temperature (77 K) after dehydration under vacuum at 673 K for 12 h using a Micromeritics Tristar 3020. The specific surface areas were evaluated using the Brunauer–Emmett–Teller (BET) method, and pore volume was measured by a single point method at p/p_0 = 0.99. Thermogravimetric (TG) analysis was carried out in a thermogravimetric analyzer (DT Q600, TA Instruments, Universal V4.5A). Analysis was performed in a dry nitrogen flow of 100 cm^3 min^{-1}. The temperature was increased from 298 to 973 K at a heating rate of 5 K min^{-1}. Before TG measurement, the sample was hydrated in a chamber with 70% relative humidity at 303 K for 1 day.

2.3 Sorption experiments and IAST calculations

Vapour-phase sorption experiments with xylene isomers and ethylbenzene were carried out at 323 K using an Intelligent

Gravimetric Analyzer (IGA, Hiden Analytical Ltd) over Co-CUK-1(MW). The sample (*ca.* 35 mg) was placed in a stainless steel sample bucket of fine mesh and was outgassed to constant weight, at a pressure of $<10^{-6}$ Torr at 575 K. The liquids used to generate the vapour were degassed fully by repeated evacuation and vapour equilibration cycles of the liquid supply side of the vapour reservoir. The vapour sorption isotherms collected using each pure isomer in the range p/p_0 = 0–1 at 323 K. The Ideal Adsorbed Solution Theory (IAST) of Myers and Prausnitz[7] was used to determine the adsorption equilibrium for 4-component gas-phase equimolar *p*-xylene/*m*-xylene/*o*-xylene/ethylbenzene mixtures. The production of *p*-xylene involves the separation of 4-component equimolar *o*-xylene(1)/*m*-xylene(2)/*p*-xylene(3)/ethylbenzene(4) mixtures.[1] Using the combined selectivity/capacity metric suggested by Krishna,[8] we calculate the volumetric separation potential for preferential adsorption of *p*-xylene, and rejection of *o*-xylene, *m*-xylene, and ethylbenzene as follows:

$$\Delta Q_{(o\mathrm{X}+m\mathrm{X}+\mathrm{EthBz})/p\mathrm{X}} = (Q_{p\mathrm{X}})\frac{y_{o\mathrm{X}}+y_{m\mathrm{X}}+y_{\mathrm{EthBz}}}{1-y_{o\mathrm{X}}-y_{m\mathrm{X}}-y_{\mathrm{EthBz}}} - (Q_{o\mathrm{X}}+Q_{m\mathrm{X}}+Q_{\mathrm{EthBz}})$$

In this equation, the volumetric loadings of each of the four aromatics, Q_i, expressed in mol L^{-1} of crystalline adsorbent, are obtained by multiplying the molar loadings, q_i, by the framework density.

2.4 Molecular simulation

The intermolecular interaction and orientation of each C_8 aromatic compound within Co-CUK-1(MW) was elucidated by grand canonical Monte Carlo (GCMC) simulations. Following the general settings used in previous studies,[9–11] the DREIDING[12] and the UFF[13] force fields were used for framework structure (organic and metal parts respectively), and the OPLS-AA[14] force field was used for adsorbate molecules. Partial charges of the framework were determined using the density-derived electrostatic and chemical (DDEC) charge method,[15] which performs atomic population analysis to determine net atomic charges based on total electron density from first-principle calculation. We used Vienna *Ab initio* Simulation Package (VASP)[16] to calculate the total electron density of the 3-D periodic framework on conditions that Perdew–Burke–Ernzerhof (PBE)[17] exchange–correlation functional, projector-augmented wave (PAW) method with a plane wave up to an energy cutoff value of 500 eV, and 2 × 2 × 3 Monkhorst–Pack for sampling the reciprocal space. GCMC simulations were performed for 5 × 10^7 steps for each aromatic compound under 303 K and 25 kPa by using a 2 × 2 × 2 superstructure of the Co-CUK-1 unit-cell. The first 4 × 10^7 GCMC steps were used to equilibrate the system, resulting in the saturated state of adsorbate molecules in the 1D pores (see Fig. S1†). The subsequent 1 × 10^7 GCMC steps were used to analyze the average interaction energy between the adsorbates and the framework.

3. Results and discussion

3.1 Microwave synthesis

Co-CUK-1 was prepared using an alternative synthetic method compared to the originally reported solvothermal route.[5] As illustrated in Fig. S2,† the synthesis of Co-CUK-1 was performed in basic aqueous solution containing KOH. When the Co(II) and 2,4-pdc ligand precursor solutions were mixed, the solution pH changed from 12.8 to 8.0, and the solution changed from light pink in colour to an opaque olive slurry after approximately 20 min. When the stirred solution was allowed to rest, the slurry separated into two layers. The top layer comprised a brownish pink solution, while the bottom layer contained dark cyan precipitates. As shown in Fig. 2, the type of heating method employed had a significant impact on the crystallization of Co-CUK-1. Heating by microwave irradiation (MW) provided clear advantages over convection heating, resulting in significantly higher product yields, as well as faster crystallization. Under MW heating, crystalline Co-CUK-1(MW) was formed in 5 min, at 78% yield. In contrast, crystallization of Co-CUK-1 under convection (HT) heating required at least 10 h and resulted in lower yields (61%). The morphology of crystallites was also more uniform for Co-CUK-1(MW) samples compared to Co-CUK-1(HT) samples (Fig. S3†). The faster crystallization and higher product yields observed from microwave-assisted synthesis may be ascribed to the faster dissolution of the precursor slurry by the selective absorption of microwaves by the polar ionic reaction mixture.[18,19]

In addition to the beneficial effects of MW heating on product purity, the microwave irradiation also positively impacted the bulk crystallinity of the Co-CUK-1 material obtained. According to our previous report,[20] after degassing at 573 K, Co-CUK-1(HT) exhibited no uptake of N_2 at 77 K but showed a large uptake of CO_2 (156 cm^3 g^{-1} at 196 K and 760 Torr (101 kPa)). The original report gave a surface area of 630 m^2 g^{-1} (micropore volume, 0.26 cm^3 g^{-1}), which was estimated by fitting the BET equation to the resulting CO_2 adsorption isotherm.[20] Interestingly, we were able to obtain a type-I N_2 adsorption isotherm for the new Co-CUK-1(MW) under identical conditions (Fig. 3). The absolute N_2 capacity of Co-

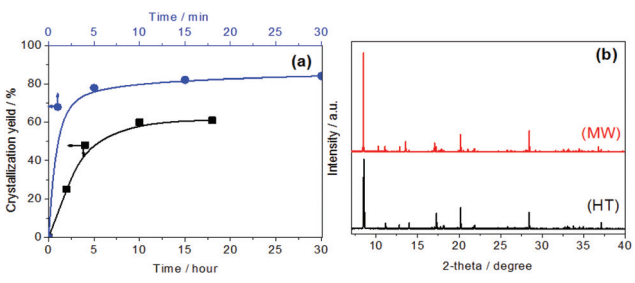

Fig. 2 (a) Crystallization yield profiles of Co-CUK-1 depending on crystallization time and synthesis method (□ hydrothermal heating; ○ microwave irradiation) and (b) XRD patterns of as-synthesized Co-CUK-1 (HT: hydrothermal heating; MW: microwave irradiation).

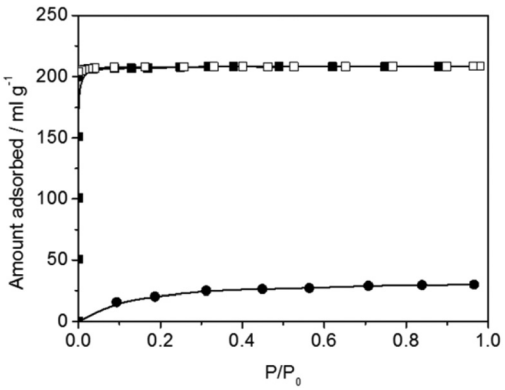

Fig. 3 Adsorption (■), desorption (□), and re-adsorption (●) isotherms of N_2 at 77 K in CUK-1(MW) degassed at 573 K under vacuum.

CUK-1(MW) (210 $cm^3\ g^{-1}$ at 77 K and 101 kPa) was also noticeably higher than that (68 $cm^3\ g^{-1}$) for Mg-CUK-1 obtained by a similar microwave method.[6] Fitting the BET equation to the N_2 isotherm gave an estimated surface area of 730 $m^2\ g^{-1}$ (micropore volume, 0.28 $cm^3\ g^{-1}$), which is about 10% higher than the value of the Co-CUK-1(HT) using the CO_2 isotherm.

Another important feature of the N_2 sorption isotherm for Co-CUK-1(MW) is that the sorption of N_2 within the CUK-1 framework revealed an irreversible type-I isotherm with a marked hysteresis (Fig. 3). Virtually no N_2 desorption was observed even when the pressure was reduced to 1 Torr. Re-adsorption of N_2 resulted in a low uptake (below 30 $cm^3\ g^{-1}$ at 760 Torr). This behaviour is similar to what was previously observed for oxygen sorption in Co-CUK-1(HT). It is a strong indication that the interaction between N_2 or O_2 and the internal pore structure was moderately strong at low temperature (77 K). To further check the effect of impurities in the 1-D channels of Co-CUK-1(HT), we collected N_2 adsorption isotherms of the conventionally prepared sample after different solvents had been used to potentially remove trapped substrates within the pores. Indeed, the N_2 adsorption–desorption isotherm obtained after immersion in dimethylformamide (DMF) and subsequent re-immersion in ethanol showed a similar uptake to that of Co-CUK-1(MW) (Fig. S4†). Comparision of the thermogravimetric analysis (TGA) profiles of the untreated and solvent-cleaned samples showed a very slight difference in weight loss (0.5%) below 673 K, which is indicative of the presence of a small quantity of residual impurities in the pores of Co-CUK-1(HT) (Fig. S5†). At present, it is not clear why the N_2 sorption uptakes at 77 K were greatly different depending on the preparation method and purification conditions, given only small differences in the TGA results. Further investigations to clarify these minor discrepancies will follow. Considering the physicochemical properties of Co-CUK-1, it is evident that the microwave method provides superior Co-CUK-1 samples with negligible pore-based impurities. Samples of Co-CUK-1(MW) were therefore suitable for testing as potentially selective adsorbents for the separation of xylenes and ethylbenzene.

3.2 Selective adsorption of *p*-xylene

Single-component equilibrium adsorption isotherms of xylene isomers and ethylbenzene in activated Co-CUK-1(MW) at 323 K (activated *in vaccuo* at 573 K for 6 h) are compared in Fig. 4. The measured pure component isotherm data for each aromatic molecule was fitted to the single-site Langmuir–Freundlich model (see ESI†). The fitted parameter values for xylene isomers and ethylbenzene are provided in Table S6.† The isotherm fits are in excellent agreement with observed data for all molecules, over the entire pressure range. The saturation capacities were determined as follows: *p*-xylene(3), $q_{3,sat}$ = 2.53; *m*-xylene(2), $q_{2,sat}$ = 1.33; *o*-xylene(3), $q_{3,sat}$ = 1.25; ethylbenzene(4), $q_{4,sat}$ = 1.73 mol kg^{-1}. It is particularly noteworthy that the saturation capacity of *p*-xylene was found to be significantly higher than that of other aromatic molecules; this is a direct reflection of the more efficient stacking of *p*-xylene molecules within the channels of Co-CUK-1. The higher saturation capacity of *p*-xylene is due to well shape-matched guest–guest stacking within the one-dimensional channels; this is apparent in the computational snapshots obtained from molecular simulations, and is also in close agreement with the actual packing structure obtained by single crystal X-ray diffraction of *p*-xylene-loaded Mg-CUK-1.[6]

We then used the Ideal Adsorbed Solution Theory (IAST) of Myers and Prausnitz[7] to determine the adsorption equilibrium for an equimolar 4-component gas mixture consisting of *p*-xylene(1), *m*-xylene(2), *o*-xylene(3), and ethylbenzene(4) (Fig. 5a). With increasing total gas pressure, the *p*-xylene loading increased at the expense of the other component molecules. It is notable that at a total pressure of 100 kPa, the adsorbed phase is significantly richer in *p*-xylene; as shown in Fig. S8,† the adsorption selectivity value approaches a value of about 50 as pore saturation is approached. The preferential adsorption of *p*-xylene, at the expense of the other C8 hydrocarbons is ascribable to entropy effects that manifest at pore saturation conditions.[1] Invoking the Boltzmann equation $S = kB\ \ln(W)$, it has been demonstrated that the com-

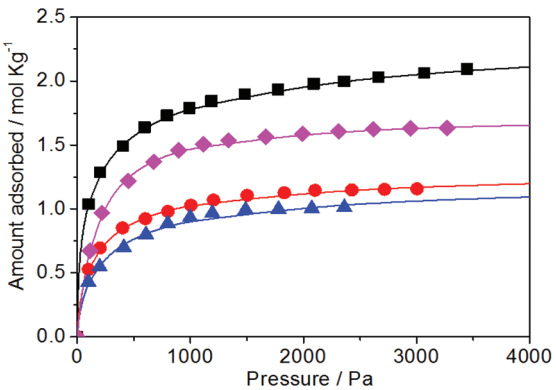

Fig. 4 Comparison of experimental data for single-component *p*-xylene (□), *m*-xylene (○), *o*-xylene (△) and ethylbenzene (◊) isotherms in Co-CUK-1(MW) with Langmuir–Freundlich fits (solid lines).

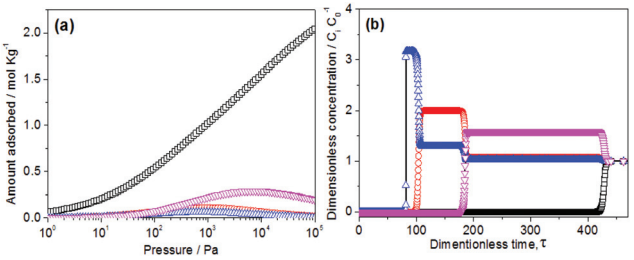

Fig. 5 (a) IAST calculations of adsorption equilibrium for equimolar gas phase 4-component *p*-xylene (□, black), *m*-xylene (○, red), *o*-xylene (△, blue) and ethylbenzene (▽, magenta) mixtures in Co-CUK-1(MW) at 303 K. (b) Transient breakthrough simulations for 4-component *p*-xylene (□, black), *m*-xylene (○, red), *o*-xylene (△, blue) and ethylbenzene (▽, magenta) mixtures in a packed bed of Co-CUK-1 operating at 303 K and 100 kPa. The inlet gas phase had partial pressures of 25 kPa for each component. Video animations showing the transient breakthroughs are available as ESI.†

ponent that packs most efficiently, *i.e.* *p*-xylene, is the one that adsorbs most strongly at pore saturation.[21]

As a next step, we compared the separation performance of Co-CUK-1(MW) with BaX, along with that of three MOFs that also exhibit high separation potential towards *p*-xylene: MAF-X8,[22] DynaMOF-100,[23,24] and the isostructural material Mg-CUK-1.[6] Adopting the methodology described in earlier work, we assessed the performances of all MOFs at conditions corresponding to pore saturation, *i.e.* $\theta_t \rightarrow 1$. Fig. 6 shows a plot of the separation potentials of each of these materials against their maximum volumetric uptakes of *p*-xylene from the 4-component mixture. A combination of high separation potential and high *p*-xylene capacity provides the best separation capability in a SMB adsorber. According to Fig. 6, the best separation performance was achieved by DynaMOF-100. The next best performance was that of Co-CUK-1(MW).

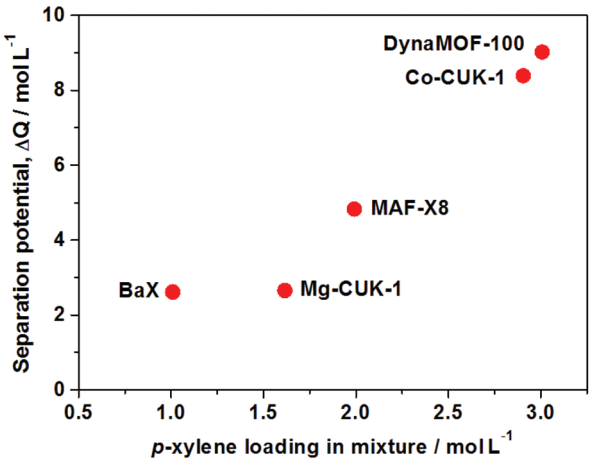

Fig. 6 Plot of separation potential (ΔQ) *vs.* *p*-xylene uptake capacity at $\theta_t \approx 1$ for various materials. The plotted value for Co-CUK-1 is from this work. The data for BaX, Mg-CUK-1, MAF-X8, and DynaMOF-100 are taken from the evaluation studies of Krishna and co-workers.[26]

3.3 Transient breakthrough simulations

Using the pure component isotherm fits to the experimental data, we carried out transient breakthrough simulations for Co-CUK-1(MW) using the methodology described in earlier works.[25,26] Fig. 5b shows the results of transient breakthrough simulations of a 4-component equimolar *p*-xylene(1)/*m*-xylene(2)/*o*-xylene(3)/ethylbenzene(4) mixture with a step input, p_i = 25 kPa for each hydrocarbon; this particular choice of partial pressures, p_i, ensures that the conditions correspond to pore saturation (*cf.* Fig. S7†). This mixture composition was chosen to enable comparisons with other MOFs reported in the published literature.[8,22,24] The breakthrough sequence obtained is *o*-xylene first, followed by *m*-xylene, ethylbenzene, and finally *p*-xylene; this sequence is essentially a reflection of the hierarchy of saturation capacities. Video animations showing the transient breakthroughs are available as in the ESI.†

3.4 GCMC simulations

To elucidate the intermolecular interaction and orientation of each C_8 aromatic compound within Co-CUK-1(MW), we also performed grand canonical Monte Carlo (GCMC) simulations. Fig. 7 shows the final snapshots of GCMC trajectories for different C_8 aromatic compounds, where the adsorbate molecules were saturated within 1-D pores of the framework (4 adsorbate molecules per Co-CUK-1 unit-cell). GCMC suggests that *p*-xylene molecules developed a well-defined head-to-tail molecular packing arrangement along the pore axis, while the packing of pure *o*-xylene, *m*-xylene, or ethylbenzene adsorbates were more frustrated; this is not surprising considering the lower symmetry of the latter adsorbates that prevents simple organization of these molecules into ordered 1-D stacks. The average interaction energy per molecule provides further insight into how Co-CUK-1(MW) offers a channel topology and atomistic environment that is most suitable to *p*-xylene adsorption. As shown in Table S9,† the average interaction energy of *p*-xylene is −22.13 kcal per mol per molecule, around 10% larger than for the other adsorbates, which yielded interaction energies in the range −20.58 to −20.63 kcal per mol per molecule. Considering that the highly polarizable μ_3-OH groups are

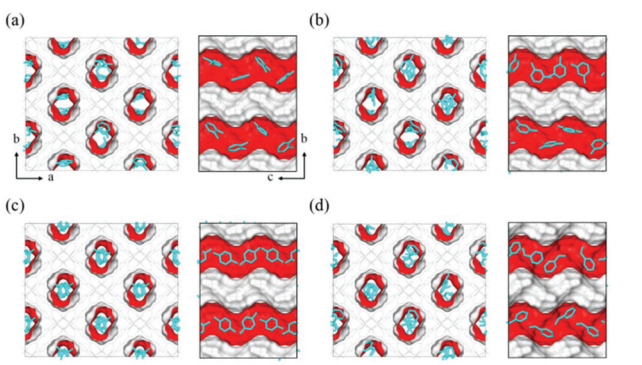

Fig. 7 Snapshots showing the molecular configuration of C_8 aromatic hydrocarbons such as (a) *o*-xylene, (b) *m*-xylene, (c) *p*-xylene, and (d) ethylbenzene within 6.8 Å channels of Co-CUK-1.

accessible to guest molecules within the corrugated pore channel (Fig. S10†), two *para*-positioned methyl functional groups are predicted to result in the most optimal molecular geometry to enable electrostatic interactions toward two μ_3-OH groups. This particular interaction is not achievable for *o*- and *m*-substituted guest adsorbates. Overall, the formation of favorable electrostatic framework-to-adsorbate (host–guest) interactions *via* the interplay of charge distribution, as well as the matching of pore topology with the chemical topology of particular adsorbates, are undoubtedly important additive factors that lead to the observed ability of CUK-1 materials to preferentially adsorb *p*-xylene from mixtures of C_8 aromatic compounds.

4. Conclusions

Microwave synthesis has been found to provide high-quality crystalline samples of Co-CUK-1 that can be used as a sorbent for the direct separation of *p*-xylene from crude mixtures of C_8 aromatic hydrocarbons. The sorption selectivity of Co-CUK-1 (MW) was shown to strongly favor *p*-xylene because adsorption of this isomer resulted in a well-defined molecular packing arrangement along the 1-D channel. In contrast, ordered packing of *o*-xylene, *m*-xylene, or ethylbenzene was more difficult to achieve as a result of poorer host–guest size and shape matching. Importantly, Co-CUK-1(MW) has clear selectivity and capacity advantages over BaX. The question of whether CUK-1(MW) (or indeed, DynaMOF-100) has true commercial potential will be answered through subsequent process development work, including breakthrough experiments, long term stability testing, and the demonstration of product desorption using co-eluents such as toluene.

Conflicts of interest

The authors have no conflicting interests.

Acknowledgements

We would like to acknowledge the financial support from the Center for Hybrid Interface Materials (HIM) for the Global Frontier R&D Program (2013M3A6B1073298, 2013M3A6B1078884) and DRC Program (SKM-1503), funded by the Ministry of Science, ICT & Future Planning, and the Welch Foundation (F-1738).

Notes and references

1 R. Krishna, *Phys. Chem. Chem. Phys.*, 2015, **17**, 39–59.
2 (*a*) G. Férey, *Chem. Soc. Rev.*, 2008, **37**, 191–214; (*b*) T. Uemura, N. Yanai and S. Kitagawa, *Chem. Soc. Rev.*, 2009, **38**, 1228–1236; (*c*) D. J. Tranchemontagne, J. L. Mendoza-Cotés, M. O'Keeffe and O. M. Yaghi, *Chem. Soc. Rev.*, 2009, **38**, 1257–1283.
3 (*a*) K. Sumida, D. L. Rogow, J. A. Mason, T. M. McDonald, E. D. Bloch, Z. R. Herm, T.-H. Bae and J. R. Long, *Chem. Rev.*, 2012, **112**, 724–781; (*b*) H. Wu, Q. Gong, D. H. Olson and J. Li, *Chem. Rev.*, 2012, **112**, 836–868.
4 B. V. de Voorde, B. Bueken, J. Denayer and D. De Vos, *Chem. Soc. Rev.*, 2014, **43**, 5766–5788.
5 S. M. Humphrey, J.-S. Chang, S. H. Jhung, J. W. Yoon and P. T. Wood, *Angew. Chem., Int. Ed.*, 2007, **46**, 272–275.
6 B. Saccoccia, A. M. Bohnsack, N. W. Waggoner, K. H. Cho, J. S. Lee, D.-Y. Hong, V. M. Lynch, J.-S. Chang and S. M. Humphrey, *Angew. Chem., Int. Ed.*, 2015, **54**, 5394–5398.
7 A. L. Myers and J. M. Prausnitz, *AIChE J.*, 1965, **11**, 121–130.
8 R. Krishna, *RSC Adv.*, 2017, **7**, 35724–35737.
9 E. García-Pérez, J. Gascón, V. Morales-Flórez, J. M. Castillo, F. Kapteijn and S. Calero, *Langmuir*, 2009, **25**, 1725–1731.
10 A. Ö. Yazaydin, R. Q. Snurr, T.-H. Park, K. Koh, J. Liu, M. D. LeVan, A. I. Benin, P. Jakubczak, M. Lanuza, D. B. Galloway, J. J. Low and R. R. Willis, *J. Am. Chem. Soc.*, 2009, **131**, 18198–18199.
11 A. Torres-Knoop, J. Heinen, R. Krishna and D. Dubbeldam, *Langmuir*, 2015, **31**, 3771–3778.
12 S. L. Mayo, B. D. Olafson and W. A. Goddard, *J. Phys. Chem.*, 1990, **94**, 8897–8909.
13 A. K. Rappe, C. J. Casewit, K. S. Colwell, W. A. Goddard and W. M. Skiff, *J. Am. Chem. Soc.*, 1992, **114**, 10024–10035.
14 W. L. Jorgensen, D. S. Maxwell and J. Tirado-Rives, *J. Am. Chem. Soc.*, 1996, **118**, 11225–11236.
15 T. A. Manz and D. S. Sholl, *J. Chem. Theor. Comput.*, 2012, **8**, 2844–2867.
16 G. Kresse and J. Furthmüller, *Comput. Mater. Sci.*, 1996, **6**, 15–50.
17 J. P. Perdew, K. Burke and M. Ernzerhof, *Phys. Rev. Lett.*, 1996, **77**, 3865–3868.
18 (*a*) S. H. Jhung, J. H. Lee and J.-S. Chang, *Bull. Korean Chem. Soc.*, 2005, **26**, 880–881; (*b*) S. H. Jhung, J. H. Lee, P. M. Forster, G. Férey, A. K. Cheetham and J.-S. Chang, *Chem. – Eur. J.*, 2006, **12**, 7899–7905; (*c*) S. H. Jhung, J.-H. Lee, J. W. Yoon, C. Serre, G. Férey and J.-S. Chang, *Adv. Mater.*, 2007, **19**, 121–124.
19 (*a*) Z. Ni and R. I. Masel, *J. Am. Chem. Soc.*, 2006, **128**, 12394–12395; (*b*) N. A. Khan and S. H. Jhung, *Cryst. Growth Des.*, 2010, **10**, 1860–1865; (*c*) E. Haque, N. A. Khan, C. M. Kim and S. H. Jhung, *Cryst. Growth Des.*, 2011, **11**, 4413–4421.
20 J. W. Yoon, S. H. Jhung, Y. K. Hwang, S. M. Humphrey, P. T. Wood and J.-S. Chang, *Adv. Mater.*, 2007, **19**, 1830–1834.
21 R. Krishna and J. M. van Baten, *Phys. Chem. Chem. Phys.*, 2017, **19**, 20320–20337.
22 A. Torres-Knoop, R. Krishna and D. Dubbeldam, *Angew. Chem., Int. Ed.*, 2014, **53**, 7774–7778.
23 S. Mukherjee, B. Joarder, B. Manna, A. V. Desai, A. K. Chaudhari and S. K. Ghosh, *Sci. Rep.*, 2014, **4**, 5761.
24 S. Mukherjee, B. Joarder, A. V. Desai, B. Manna, R. Krishna and S. K. Ghosh, *Inorg. Chem.*, 2015, **54**, 4403–4408.
25 R. Krishna, *RSC Adv.*, 2015, **5**, 52269–52295.
26 R. Krishna, *Microporous Mesoporous Mater.*, 2014, **185**, 30–50.

SUPPORTING INFORMATION:

Highly Selective Adsorption of *p*-Xylene over other C_8 Aromatic Hydrocarbons by Co-CUK-1: A Combined Experimental and Theoretical Assessment

Ji Woong Yoon,[+][a] Ji Sun Lee,[+][a,b] Graham W. Piburn,[c] Kyoung Ho Cho,[a] Keonghee Jeon,[d] Hyung-Kyu Lim,[d] Hyungjun Kim,[d] Chul-Ho Jun,[b] Simon M. Humphrey,[c] Rajamani Krishna*[e] and Jong-San Chang*[a,f]*

[a] *Research Center for Nanocatalysts, Korea Research Institute of Chemical Technology (KRICT), P.O.Box 107, Yusung, Daejeon 305-600, Korea. Email: jschang@krict.re.kr*

[b] *Department of Chemistry, Center for Bioactive Molecular Hybrid, Yonsei University, Seodamoonku, Seoul 120-749, Korea*

[c] *Department of Chemistry, the University of Texas at Austin, 2.204 Welch Hall, 105 E. 24th St. Stop A5300, Austin TX 78712, U.S.A. Email: smh@cm.utexas.edu*

[d] *Graduate School of Energy, Environment, Water, and Sustainability; Korea Advanced Institute of Science and Technology (KAIST), Daehak-ro 291, Yuseong-gu, Daejeon 305-701, Korea*

[e] *Van't Hoff Institute for Molecular Sciences, University of Amsterdam, Science Park 904, Amsterdam 1098 XH, The Netherland. Email: r.krishna@contact.uva.nl*

[f] *Department of Chemistry, Sungkyunkwan University, Suwon 440-476, Korea*

[+] *These two authors equally contributed to this work.*

Contents

Fitting of pure component isotherms in Co-CUK-1

The measured pure component isotherm data for each aromatic molecule was fitted with the single-site Langmuir-Freundlich model:

$$q = q_{sat}\frac{bp^{\nu}}{1+bp^{\nu}} \tag{1}$$

The saturation capacities q_{sat}, Langmuir- constants b, and the Freundlich exponent ν, are provided in Table S5. It provides a comparison of the experimental isotherm data with the Langmuir-Freundlich fits. The fits are excellent for all four guest molecules.

Let us define, $q_{i,sat}$, as the saturation capacity of species i. The saturation capacities are determined to be:

p-xylene(1), $q_{1,sat}$ = 2.53 mol kg^{-1}

m-xylene(2), $q_{2,sat}$ = 1.33 mol kg^{-1}

o-xylene(3), $q_{3,sat}$ = 1.25 mol kg^{-1}

ethylbenzene(4), $q_{4,sat}$ = 1.73 mol kg^{-1}

IAST calculations of mixture adsorption equilibrium in Co-CUK-1

We use the Ideal Adsorbed Solution Theory (IAST) of Myers and Prausnitz[1] to determine the adsorption equilibrium for equimolar gas phase 4-component equimolar *p*-xylene(1)/*m*-xylene(2)/*o*-xylene(3)/ethylbenzene(4) mixtures; see Figure 4(a) With increasing total gas pressure, the *p*-xylene loading increases at the expense of its partner molecules. We note that at a total pressure of 100 kPa, the adsorbed phase is rich in *p*-xylene.

Let us define the fractional occupancy within the pores, θ_t

$$\theta_t = \sum_{i=1}^{n}\frac{q_i}{q_{i,sat}} \tag{2}$$

where q_i is the molar loading of species i in the mixture, and $q_{i,sat}$ is the saturation capacity of species i.

Figure S6 shows the calculations of the fractional occupancy, θ_t, within the pores of Co-CUK-1 as a function of the total gas phase pressure, p_t. We note that the pores are saturated, i.e. $\theta_t \to 1$, when the total pressure p_t reaches 100 kPa.

For separation of 4-component equimolar *p*-xylene(1)/*m*-xylene(2)/*o*-xylene(3) /ethylbenzene(4) mixtures we adopt the following definition of selectivity that was used in the recent paper of Torres-Knoop et al.[2]

$$S_{ads} = \frac{(q_3)/(q_1+q_2+q_4)}{(p_3)/(p_1+p_2+p_4)} = 3\frac{(q_3)}{(q_1+q_2+q_4)} \tag{3}$$

Figure S7 shows that the S_{ads} value as a function of the fractional pore occupancy, θ_t. We note that the selectivity value approaches a value of about 50 as $\theta_t \to 1$. The selectivity is strongly in favor of *p*-xylene because of molecular packing effects; this principle has been elucidated in detail in earlier work.[3] The strong, near-exponential increase in the selectivity in favor of *p*-xylene selectivity is a typical characteristic of separations due to molecular packing or entropy effects.

Transient breakthrough simulations

The separation performance of a fixed-bed adsorber is dictated by both adsorption selectivity and capacity. A higher capacity to adsorb p-xylene is a desirable characteristic of SMB adsorbers. Using the pure component isotherm fits of experimental data, we carried out transient breakthrough simulations for Co-CUK-1(MW) using the methodology described in in earlier works.[4,5]

The breakthrough characteristics for any component are essentially dictated primarily by the characteristic contact time $\frac{L}{v} = \frac{L\varepsilon}{u}$ between the crystallites and the surrounding fluid phase. It is common to use the dimensionless time, $\tau = \frac{tu}{L\varepsilon}$, obtained by dividing the actual time, *t*, by the characteristic time, $\frac{L\varepsilon}{u}$ when plotting simulated breakthrough curves. For the breakthrough simulations reported here we use the parameter values: L = 0.3 m; voidage of bed, ε = 0.4; interstitial gas velocity, v = 0.1 m/s; superficial gas velocity, u = 0.04 m/s.

Notation

b	Langmuir-Freundlich constant, $\mathrm{Pa}^{-\nu}$
c_i	molar concentration of species *i* in gas mixture, mol m^{-3}
c_{i0}	molar concentration of species *i* in gas mixture at inlet to adsorber, mol m^{-3}
L	length of packed bed adsorber, m
n	number of components in the mixture, dimensionless
p_i	partial pressure of species *i* in mixture, Pa
p_t	total system pressure, Pa
q_i	component molar loading of species *i*, mol kg^{-1}
q_t	total molar loading for mixture adsorption, mol kg^{-1}
$q_{i,sat}$	molar loading of species *i* at saturation, mol kg^{-1}
Q_i	volumetric loading of species *i* at saturation, mol L^{-1}
ΔQ_i	volumetric separation capacity of species *i* from a mixture, mol L^{-1}
S_{ads}	adsorption selectivity, dimensionless

t	time, s
T	absolute temperature, K
u	superficial gas velocity in packed bed, m s^{-1}
v	interstitial gas velocity in packed bed, m s^{-1}
y_i	mole fraction of species *i* in a mixture of species, dimensionless

Greek letters

ε	voidage of packed bed, dimensionless
θ_t	fractional occupancy for mixture adsorption, dimensionless
v	exponent in dual-Langmuir-Freundlich isotherm, dimensionless
τ	time, dimensionless

Subscripts

i	referring to component *i*
t	referring to total mixture

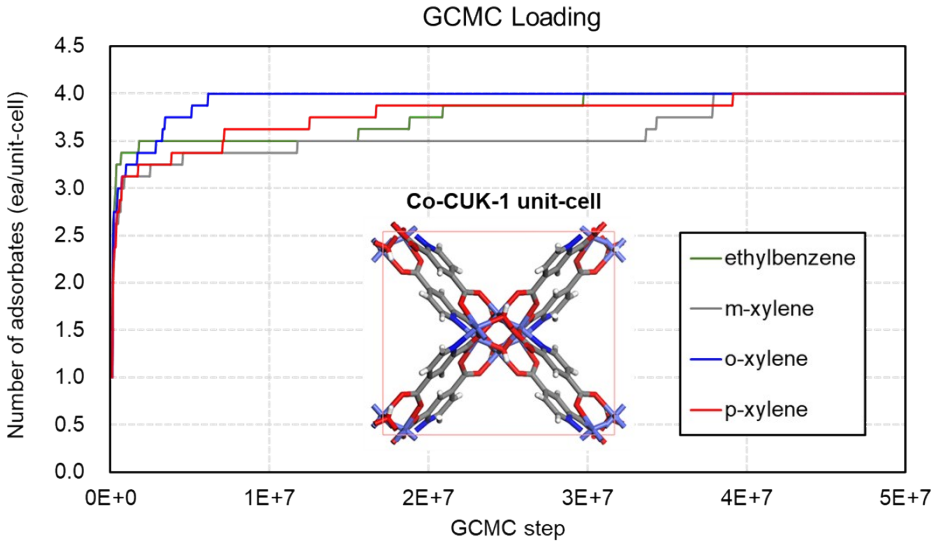

Figure S1. GCMC loading trajectory for each adsorbate molecule in Co-CUK-1 unit-cell.

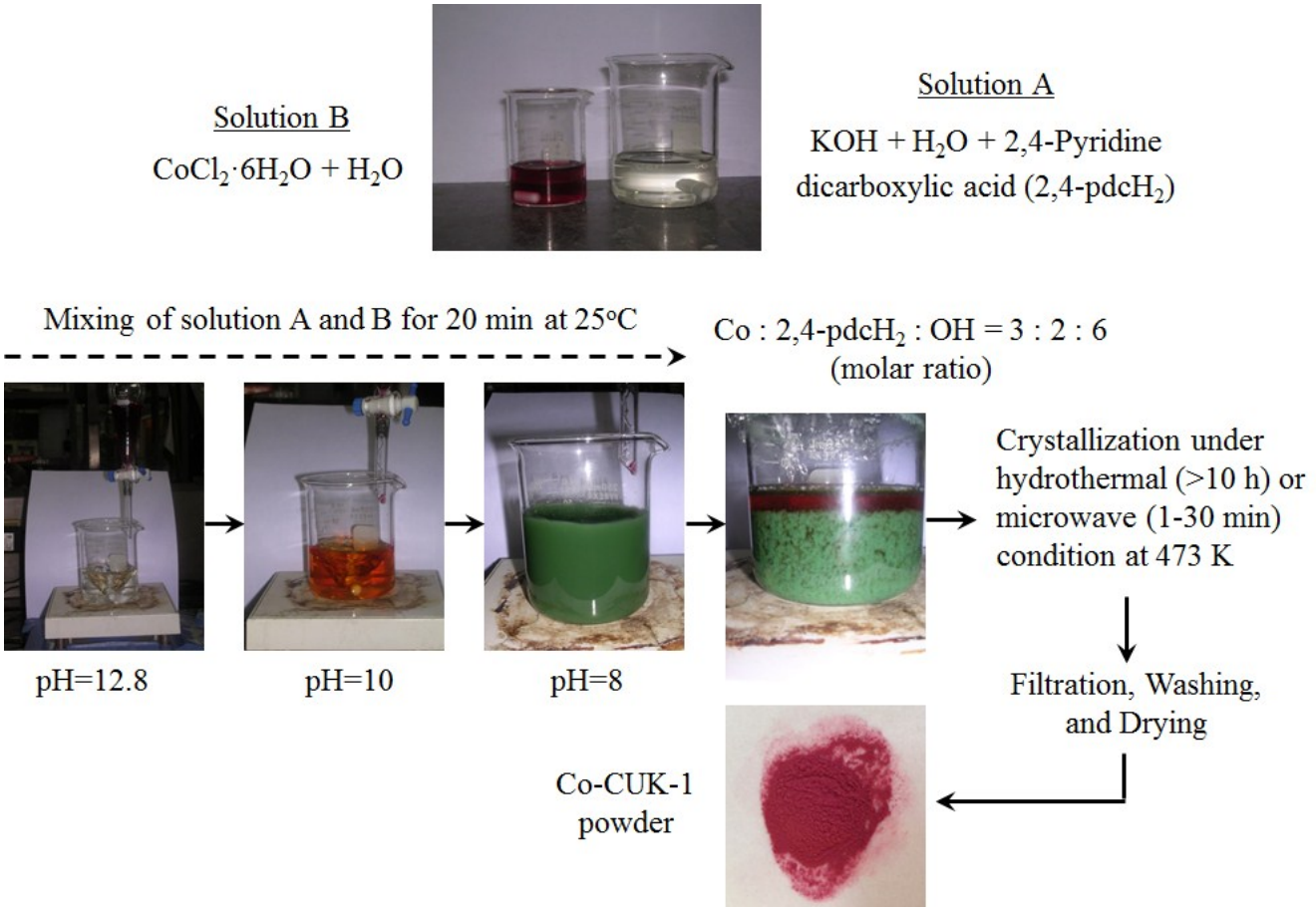

Figure S2. Stepwise pictures according to synthesis steps of Co-CUK-1.

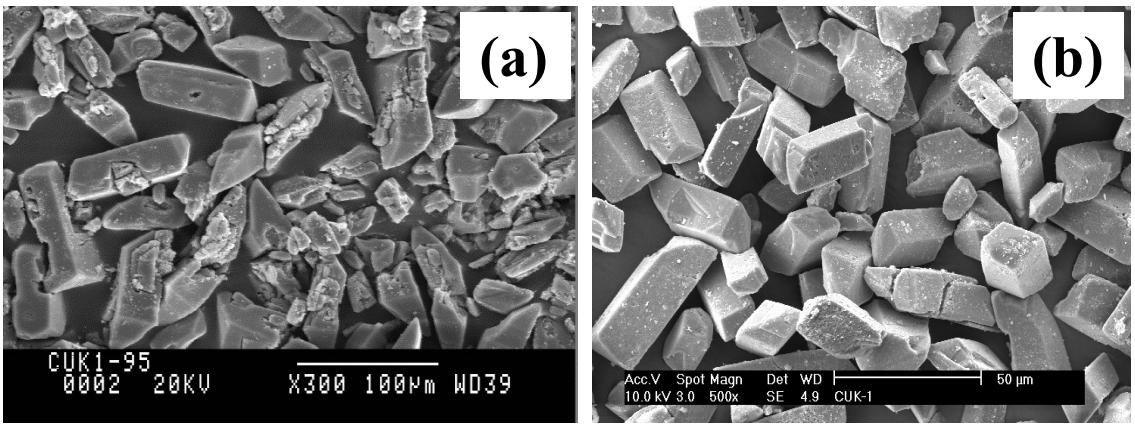

Figure S3. SEM images of (a) Co-CUK-1(HT) and Co-CUK-1(MW).

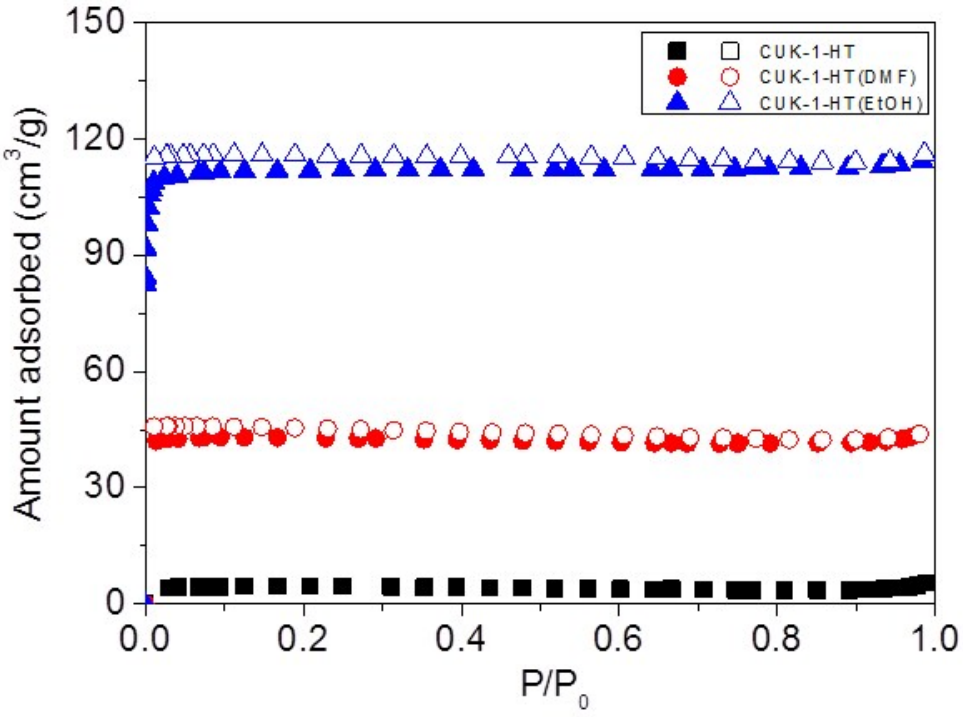

Figure S4. N_2 adsorption isotherms of Co-CUK-1(HT) at 77 K depending on purification with solvents.

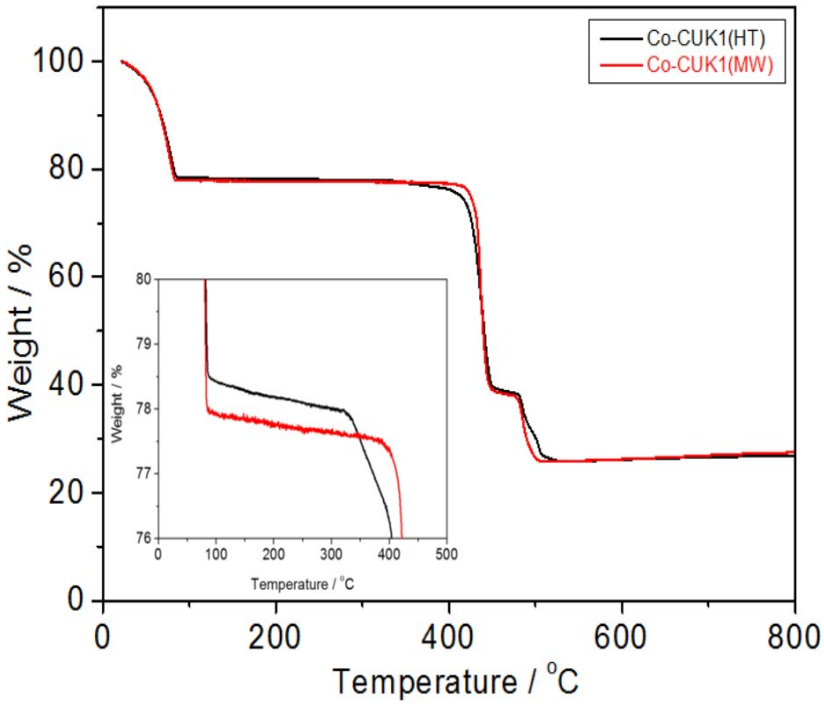

Figure S5. Thermogravimetric profiles of two Co-CUK-1 samples. An inset figure displays a larger weight loss (0.5 wt%) in Co-CUK-1(MW) than that in Co-CUK-1(HT) below 673 K.

	q_{sat} mol kg^{-1}	b Pa^{-v}	v_i dimensionless
p-xylene	2.53	5.74 x 10^{-2}	0.54
m-xylene	1.33	2.32 x 10^{-2}	0.72
o-xylene	1.25	1.79 x 10^{-2}	0.72
ethylbenzene	1.73	5.71 x 10^{-3}	1

Table S1. Langmuir-Freundlich parameters for C_8 aromatic hydrocarbons at 323 K in Co-CUK-1(MW).

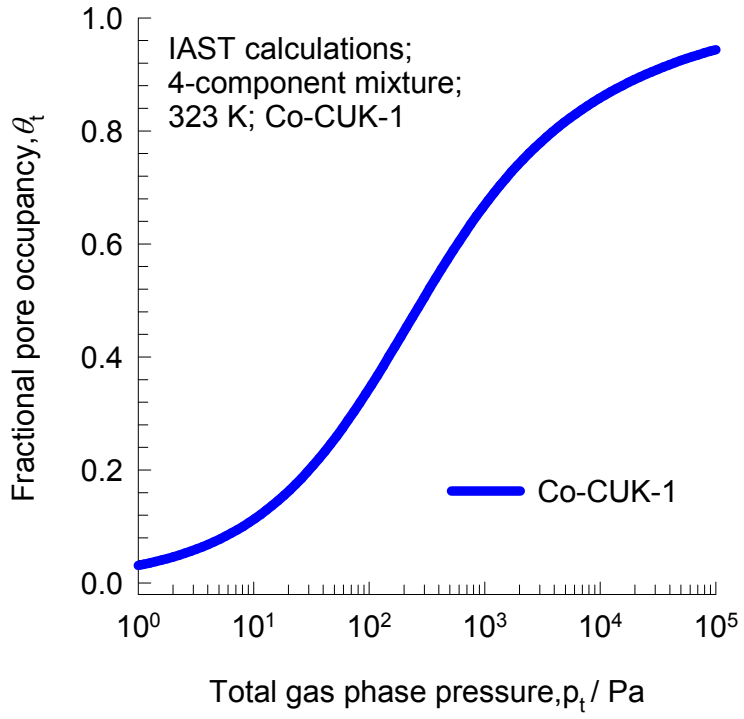

Figure S6. Calculations of the fractional occupancy, θ_t, within the pores of Co-CUK-1(MW) at 323 K as a function of the total gas phase pressure, p_t.

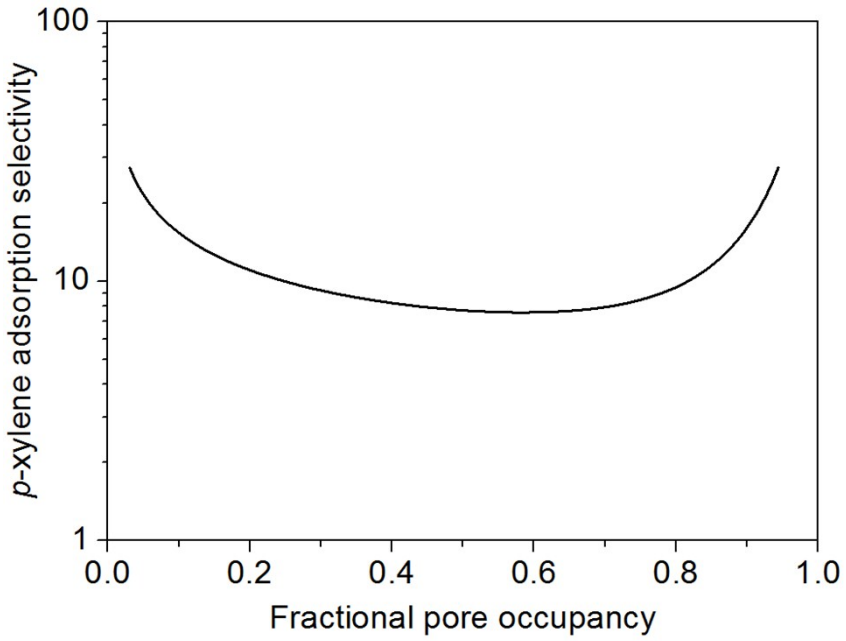

Figure S7. IAST calculations for *p*-xylene adsorption selectivity for 4-component *p*-xylene/*m*-xylene/*o*-xylene/ethylbenzene mixture in Co-CUK-1(MW) at 323 K. The *x*-axis is fractional occupancy, θ_t, within the pores of the MOFs.

Adsorbate	Average Interaction Energy (kcal/mol/molecule) Total / Electrostatic / VdW
p-Xylene	-22.13 / -20.71 / -1.42
m-Xylene	-20.63 / -19.37 / -1.26
o-Xylene	-20.60 / -19.70 / -0.91
ethylbenzene	-20.58 / -19.51 / -1.07

Table S2. Average interaction energy between adsorbate and framework.

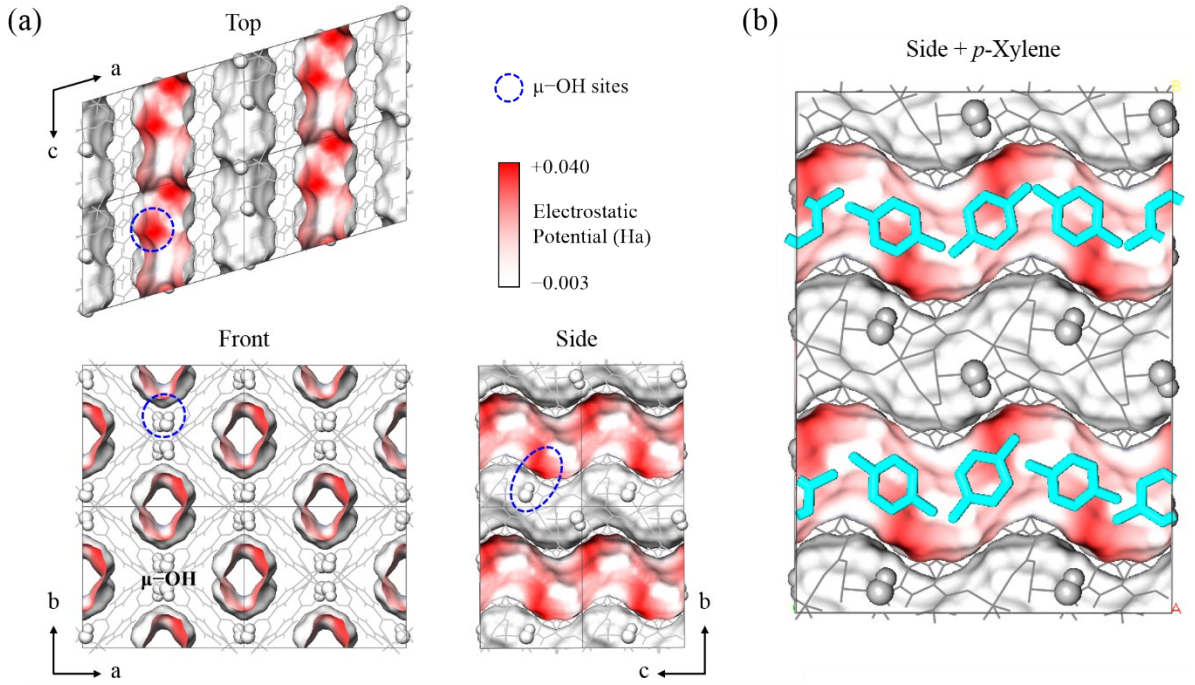

Figure S8. (a) Electrostatic potential map due to the electron density of the Co-CUK-1 framework, which shows highly polarized region due to μ-OH functional groups and (b) Chemical topology of *p*-xylene and its packing structure are suitable for developing adsorbate-framework interaction with highly polarized region.

References

1. A. L. Myers, J. M. Prausnitz, *A.I.Ch.E.J.*, 1965, **11**, 121-130.
2. A.Torres-Knoop, R. Krishna, D. Dubbeldam, *Angew. Chem. Int. Ed.*, 2014, **53**, 7774-7778.
3. R. Krishna, *Phys. Chem. Chem. Phys.*, 2015, **17**, 39-59.
4. R. Krishna, *RSC Adv.*, 2015, **5**, 52269-52295.
5. R. Krishna, *Microporous Mesoporous Mater.*, 2014, **185**, 30-50.